Supporting Information

In situ growth of active catalytic layer on the commercial stainless steel via a hydrothermal-assisted corrosion process for efficient oxygen evolution reaction

Jiuyang Xia [a, ‡], Jianghong Zhang, [b, ‡] Kang Huang [a, ‡], Bowei Zhang [a, *], Fei Wu [a], Yu Liang [b], Shuai Lu [a], Yizhong Huang [b, *], Junsheng Wu [a, *]

[a] *Institute for Advanced Materials and Technology, University of Science and Technology Beijing, Beijing, 100083, China*

[b] *School of Materials Science and Engineering, Nanyang Technological University, 50 Nanyang Avenue, 639798, Singapore.*

**Corresponding authors: Junsheng Wu*(wujs76@163.com)*; Bowei Zhang*(bwzhang@ustb.edu.cn)*; Yizhong Huang*(yzhuang@ntu.edu.sg)

‡*These authors contributed equally to this work.*

Table S1 The chemical compositions and contents of 316L SS（wt.%）.

Element	C	Si	Mn	P	S	Cr	Ni	Mo	Fe
316L	≤ 0.03	≤ 1.00	≤ 2.00	≤ 0.045	≤ 0.03	16 - 18	10 - 14	2-3	-

Process parameters

1.1 Hydrothermal temperature

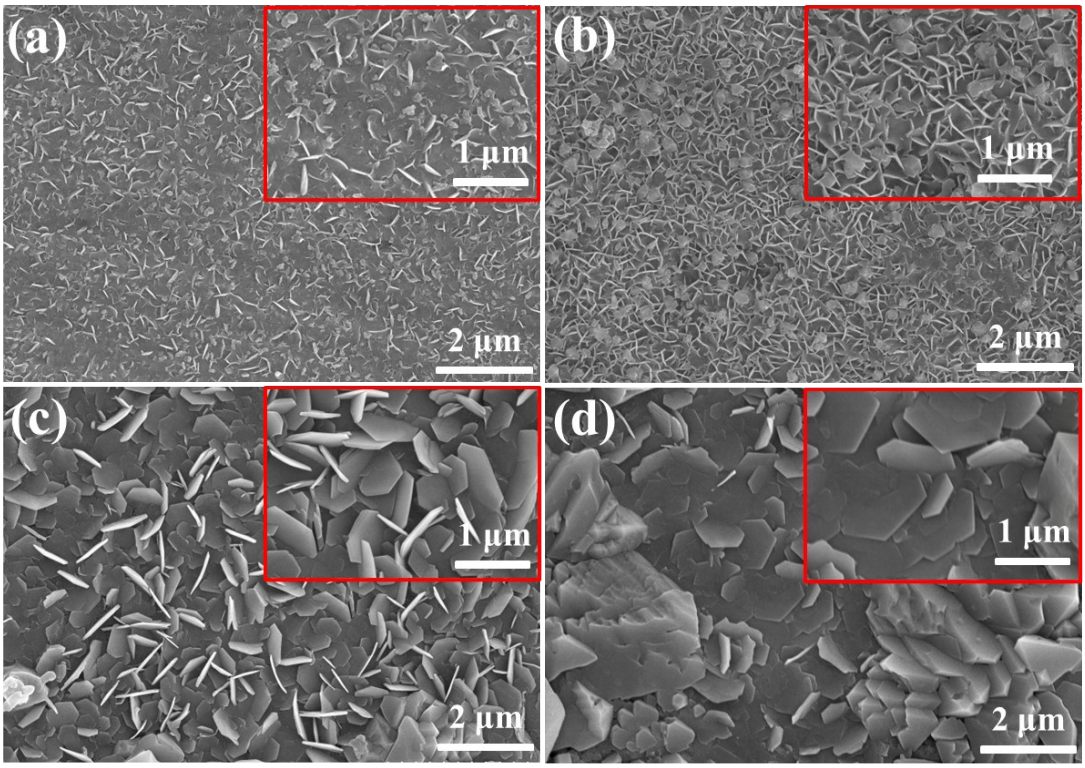

Fig. S1 SEM images of the surface of the prepared corrosion electrodes with the hydrothermal temperature((a)120 ºC, (b)150 ºC, (c)180 ºC, (d)210 ºC).

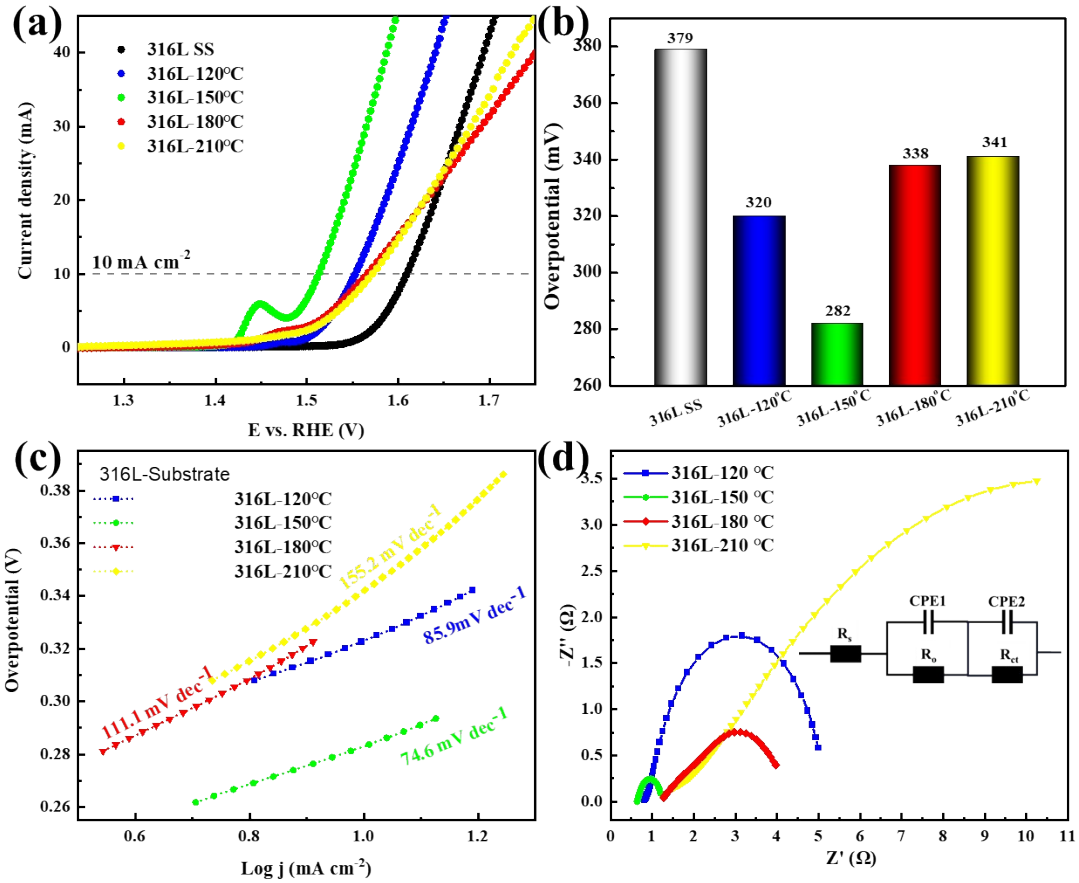

Fig. 2 (a)LSC curves, (b)Overpotentials at 10 mA cm^{-2}, (c)Tafel slops, (d)EIS curves of the 316L-bank, 316L-120 °C, 316L-150 °C, 316L-180 °C and 316L-210 °C(inset: corresponding equivalent circuit used for fitting the Nyquist plots).

1.2 NaCl concentration

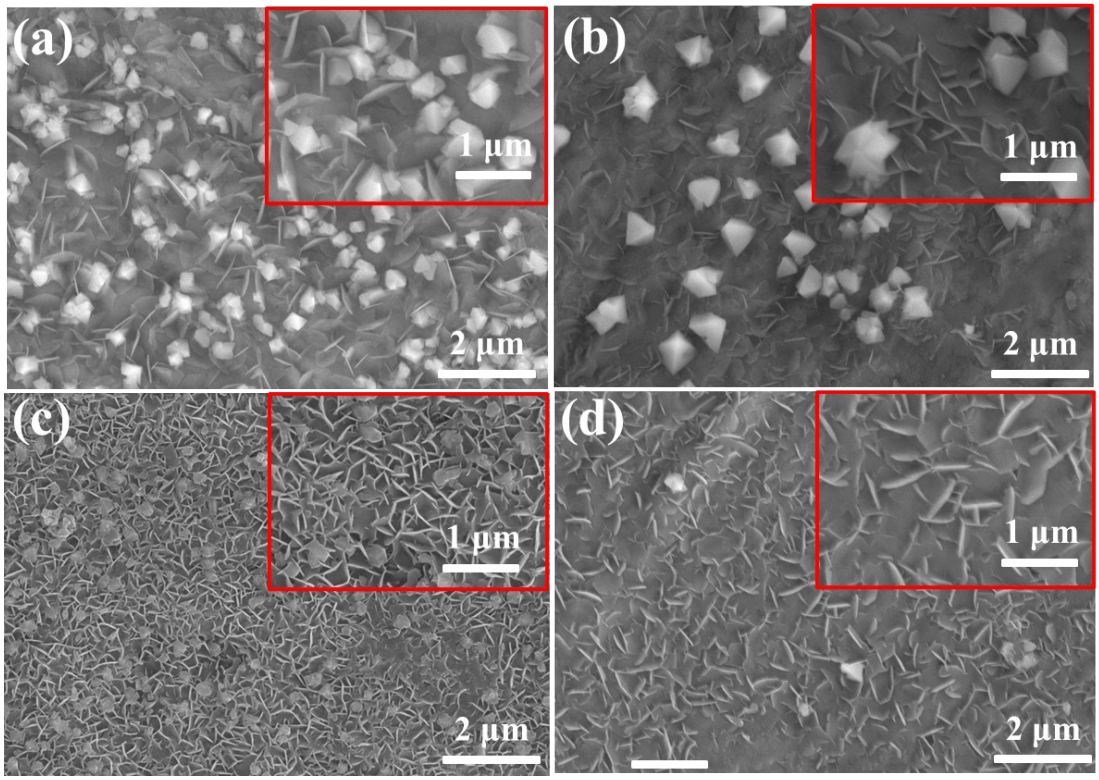

Fig. S3 SEM images of the surface of the prepared corrosion electrodes with the NaCl concentration((a)0 M, (b)0.2 M, (c)0.3 M, (d)0.4 M).

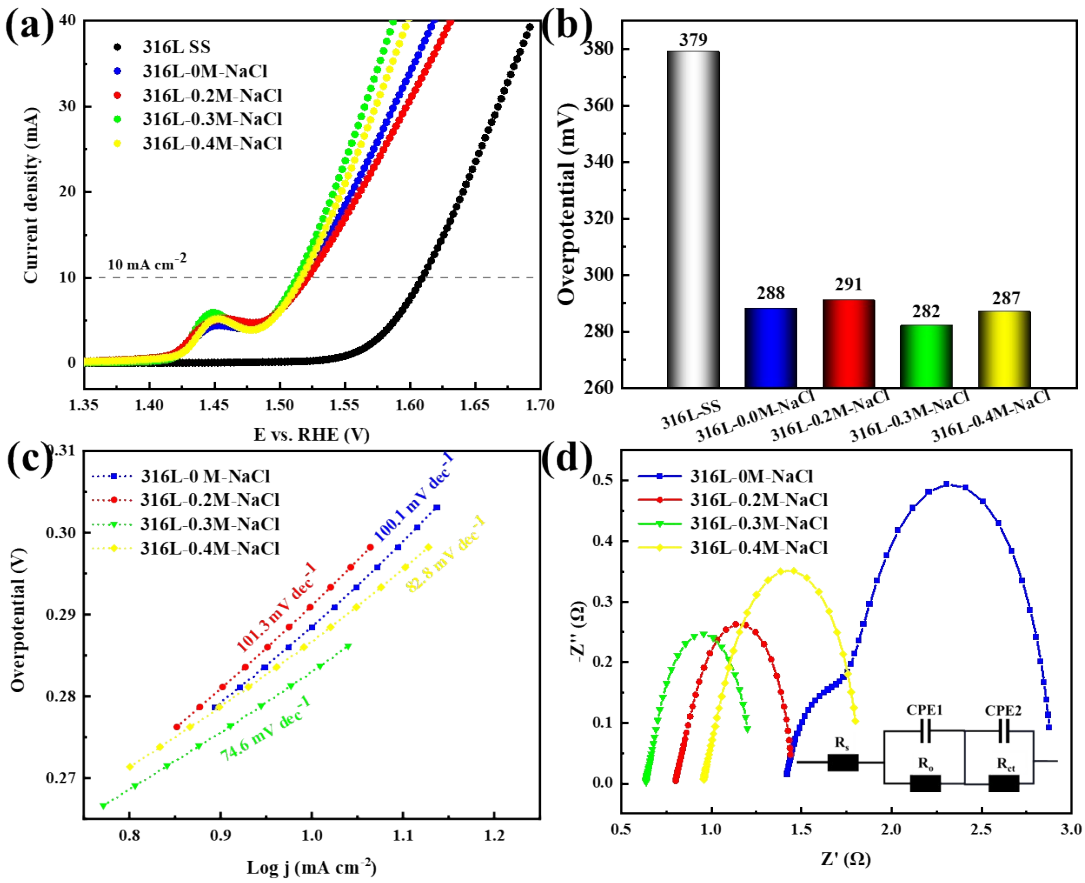

Fig. S4 (a)LSC curves, (b)Overpotentials at 10 mA cm^{-2}, (c)Tafel slops, (d)EIS curves of the 316L-SS, 316L-0M-NaCl, 316L-0.2M-NaCl, 316L-0.3M-NaCl and 316L-0.4M-NaCl (inset: corresponding equivalent circuit used for fitting the Nyquist plots).

1.3 NaOH concentration

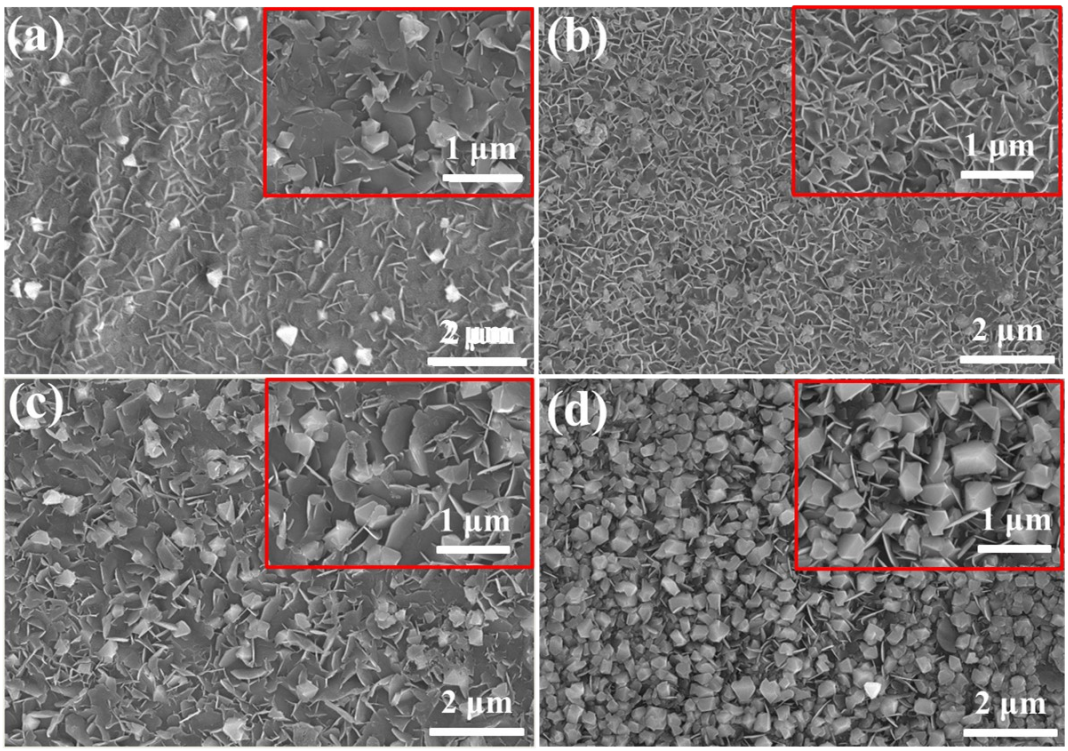

Fig. S5 SEM images of the surface of the prepared corrosion electrodes with the NaOH concentration((a)0.2 M, (b)0.3 M, (c)0.4 M, (d)0.5 M).

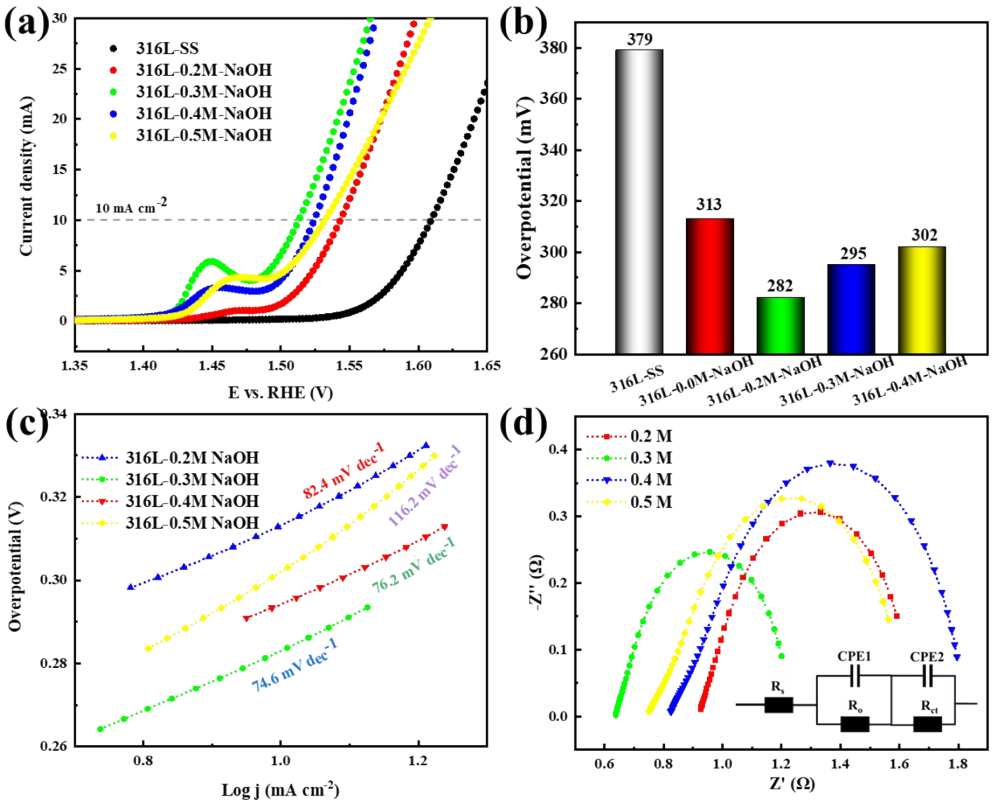

Fig. S6 (a)LSC curves, (b)Overpotentials at 10 mA cm^{-2}, (c)Tafel slops, (d)EIS curves of the 316L-SS, 316L-0.2M-NaOH, 316L-0.3M-NaOH, 316L-0.4M-NaOH and 316L-0.5M-NaOH(inset: corresponding equivalent circuit used for fitting the Nyquist plots).

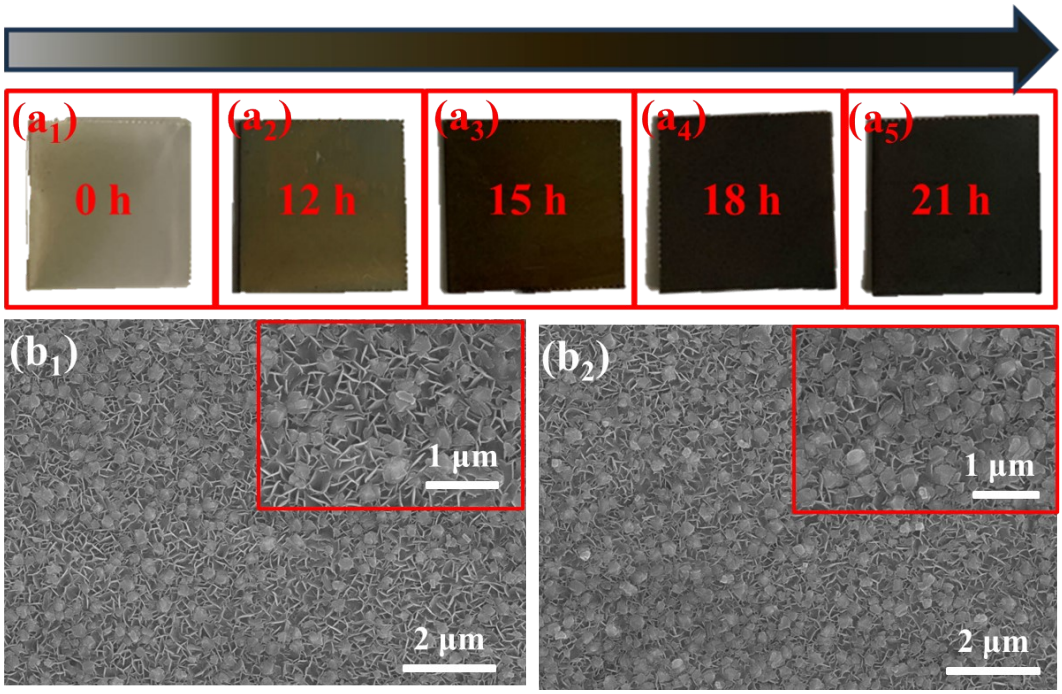

Fig. S7 (a_1-a_5)The digital images of the prepared corrosion electrodes with the hydrothermal time((a_1)0 h, (a_2)12 h, (a_3)15 h, (a_4)18 h, (a_5)21 h). (b_1-b_2)SEM images of the surface of the prepared corrosion electrodes with the corrosion time((b_1)18 h, (b_2)21 h).

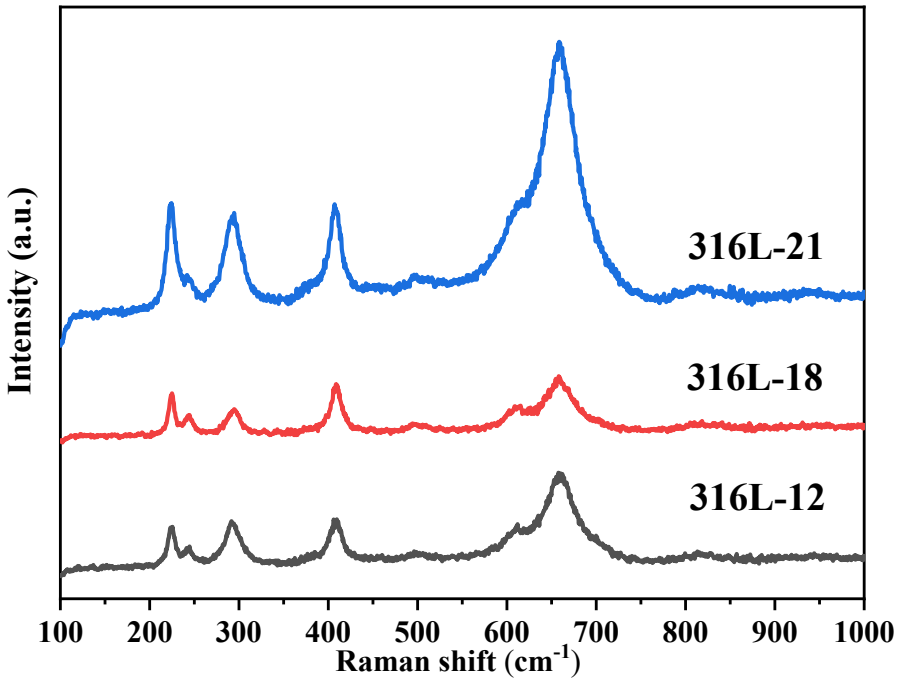

Fig. S8 Raman spectra of the 316L-12, 316L-18 and 316L-21 sample.

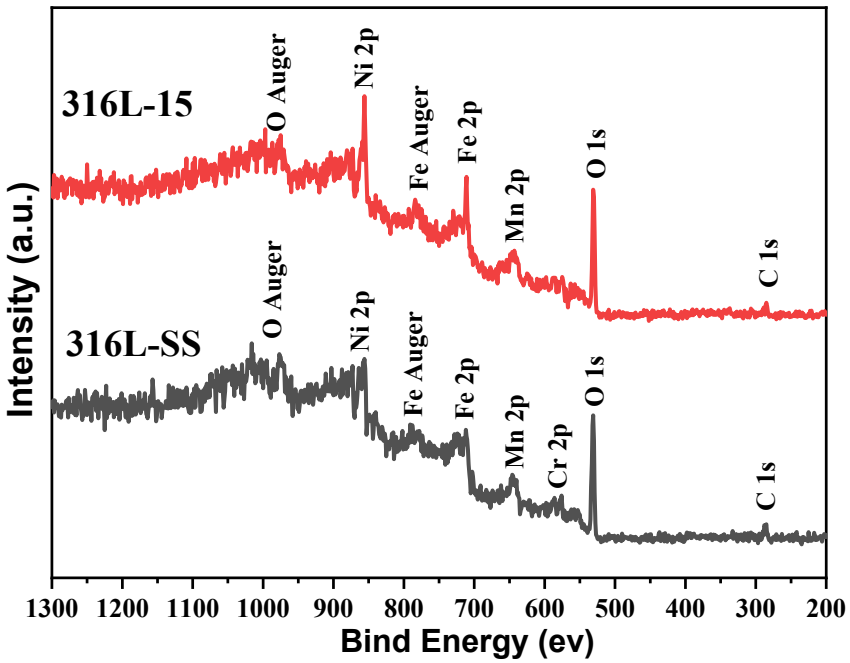

Fig. S9 XPS survey spectra of 316L-SS and 316L-15 sample

Table S2 The XPS quantitative data of $Fe(Ni)_{1.833}(OH)_{0.5}O_{2.5}$(atom.%).

Sample	XPS results	Atomic composition
$Fe(Ni)_{1.833}(OH)_{0.5}O_{2.5}$	Fe:Ni:O:OH=(0.55:0.45):(0.83:0.17)$_3$	Fe:Ni:O:OH=16:16:80:16

Table S3 Comparison of OER performance of 316L-15 with recently reported.

Materials	Methode	Current density (mV cm^{-1})	η_{10} (mV)	Ref.
316L-15	Corrosion	10	282	This work
316L-SS	directly use	10	370	[47]
Ni(Fe)O_xH_y/SSNNi	hydrothermal	20	310	[20]
AT-316L-SS	additively manufactured	10	310	[22]
304-SS	etch- thermal annealing	10	370	[17]
SSFF	chemical etch	10	300	[19]
AISI 304	chemical oxidation	10	300	[18]
316L-SS	electro-oxidation	10	300	[3]
304-SS	cathodic plasma	10	323	[21]
3D-CSS	3D-printed	10	302	[48]
SS304	Etched and anodized	10	343	[49]
SS434 scrubber	bare	10	418	[50]
SS304 foil	anodization	10	310	[51]
SS235	Chlorinated	10	347	[52]

Table S4 The corresponding components parameters values were obtained by fitting the Nyquist plots.

Elements / Samples	R_s (Ω)	R_o (mΩ)	CPE1		R_{ct} (Ω)	CPE2		χ^2 (%)
			Y_0 (mMh_0*s^N)	N		Y_0 (mMh_0*s^N)	N	
316L-12	0.69	133	318	0.606	1.08	31.5	0.958	0.23
316L-15	0.64	55.5	209	0.688	0.53	59.8	0.934	0.15
316L-18	0.67	122	722	0.546	1.13	85.0	0.948	0.19
316L-21	0.86	177	576	0.649	1.24	93.4	0.966	0.30

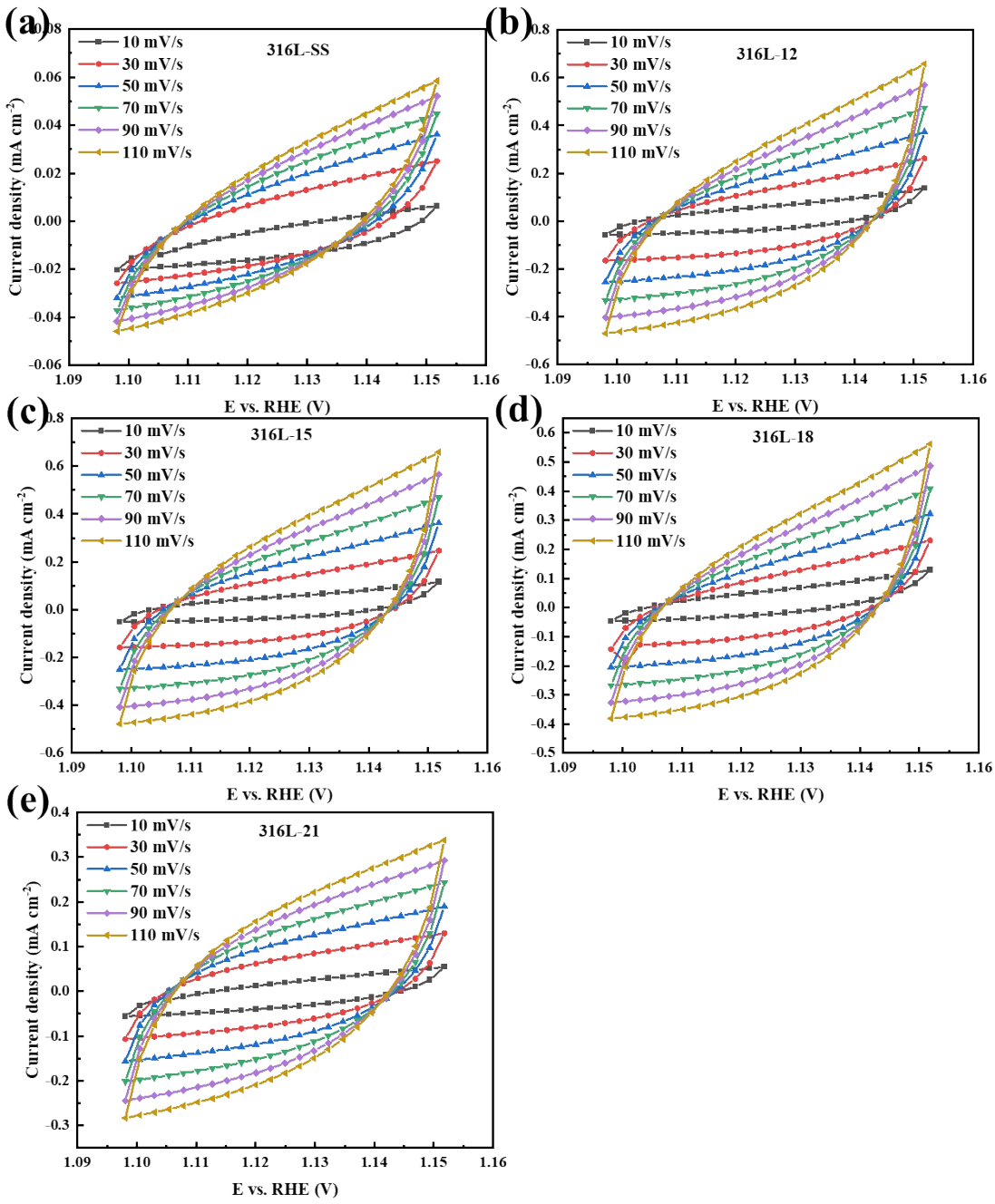

Fig. S10 Cyclic voltammograms of (a) 316L-SS, (b) 316L-12, (c)316L-15, (d)316L-18 and (e)316L-21 at the scan rate of 10 mV s^{-1}, 30 mV s^{-1}, 50 mV s^{-1}, 70 mV s^{-1}, 90 mV s^{-1} and 11070 mV s^{-1}, respectively.

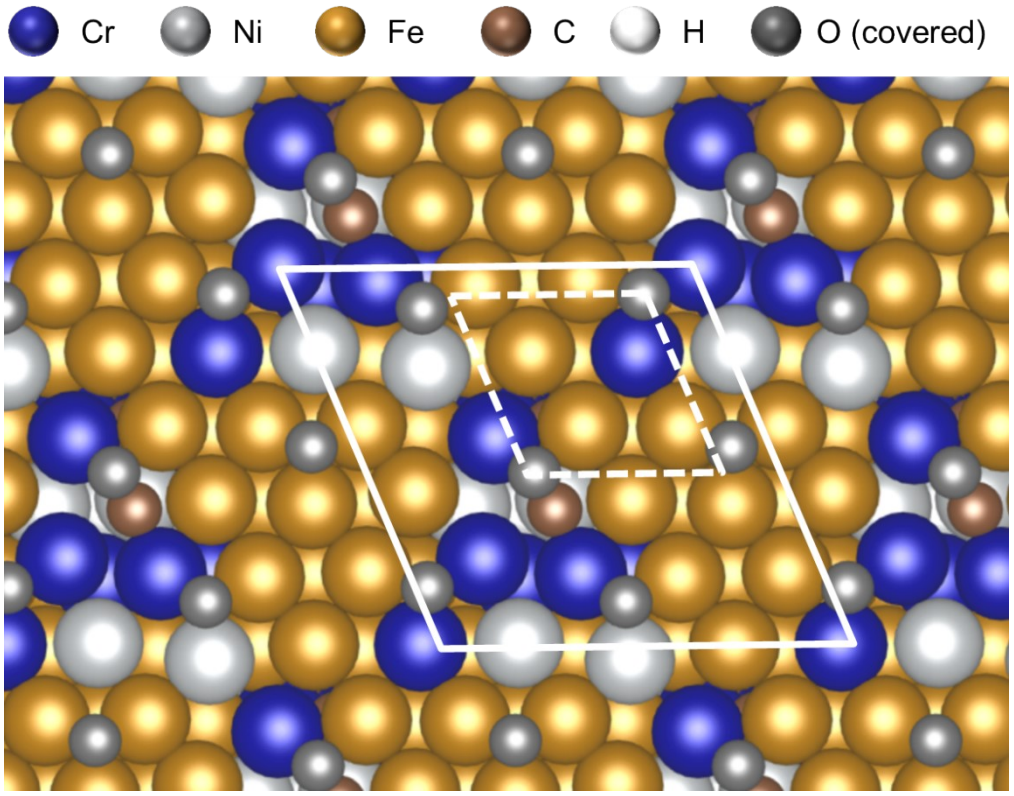

Fig. S11 the model of the Ni-incorporated $Fe_{1.833}(OH)_{0.5}O_{2.5}$

Table S5 The corresponding free energy values of different intermediates

△G / Model	△G(OH*)	△G(O*)	△G(OOH*)	△G(M*+O2)
Cr_2O_3	0.63	0.12	4.07	4.91
Fe@FeNiOOH	3.17	4.93	5.52	4.91
Ni@FeNiOOH	2.52	4.07	4.75	4.91
CrFeNiC	0.66	0.99	4.66	4.91

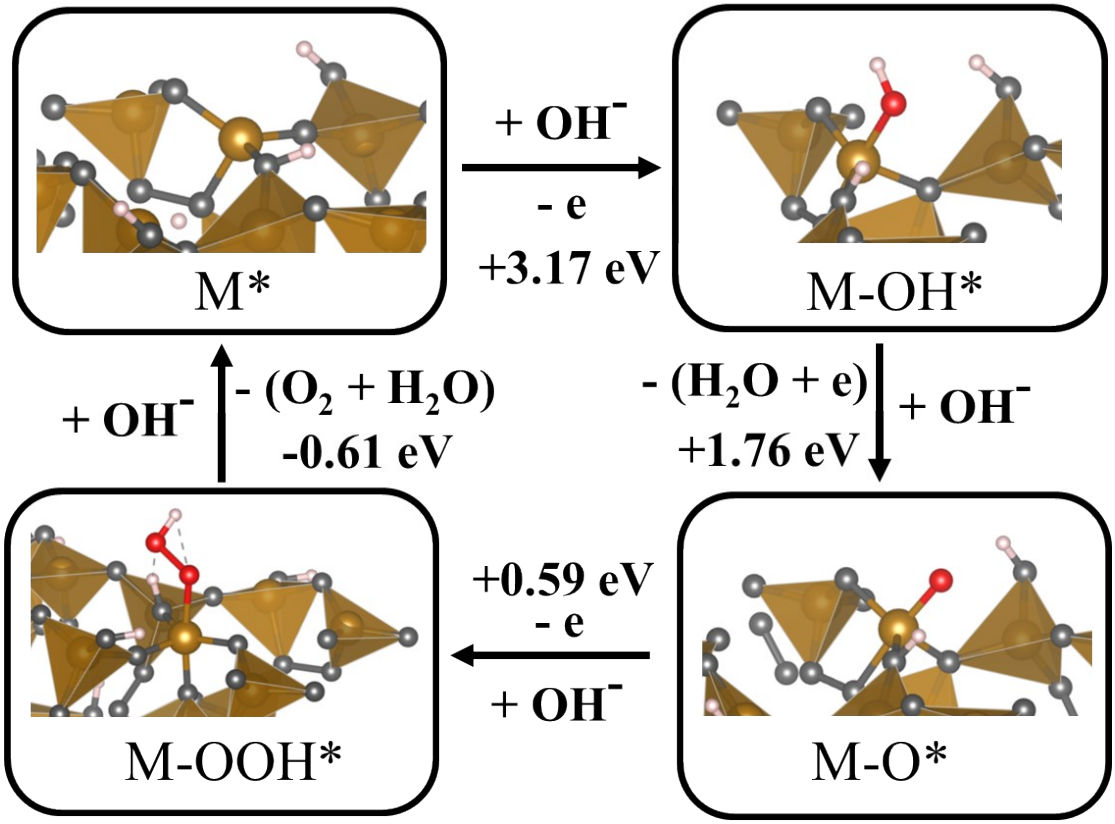

Fig. S12 DFT The reaction diagram of the pour $Fe_{1.833}(OH)_{0.5}O_{2.5}$.

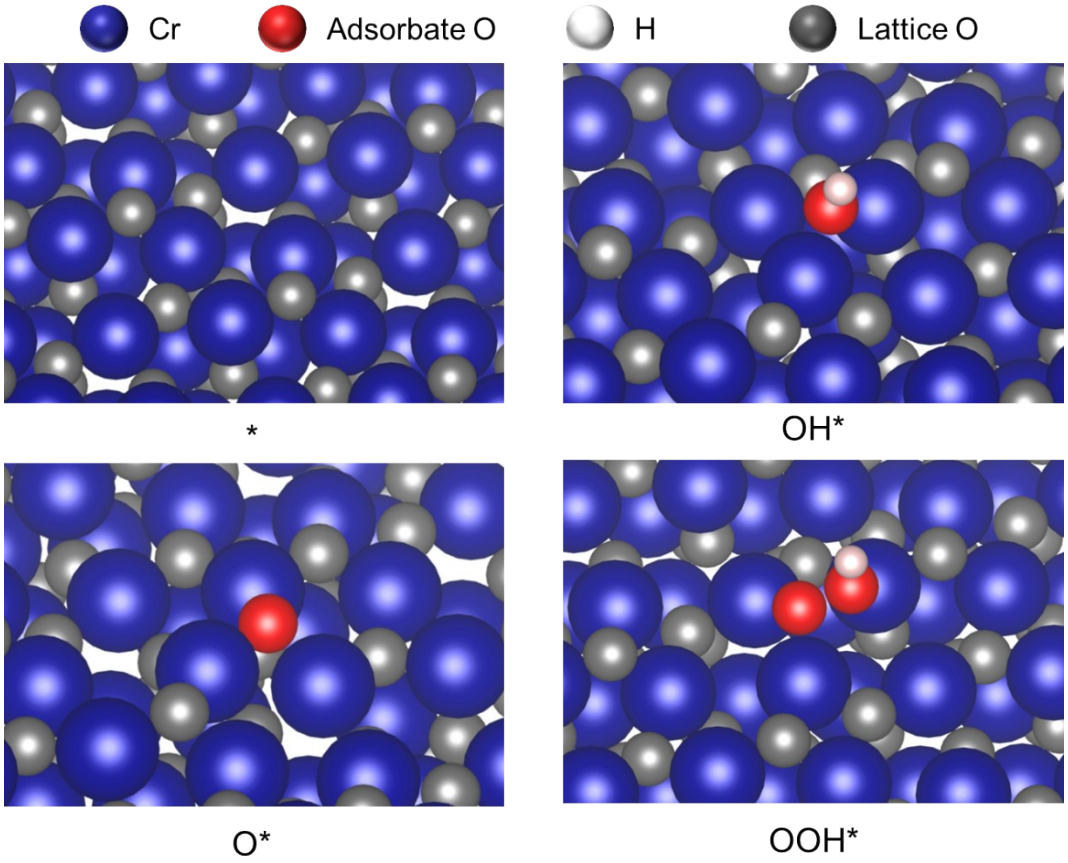

Fig. S13 DFT The reaction diagram of the Cr_2O_3.

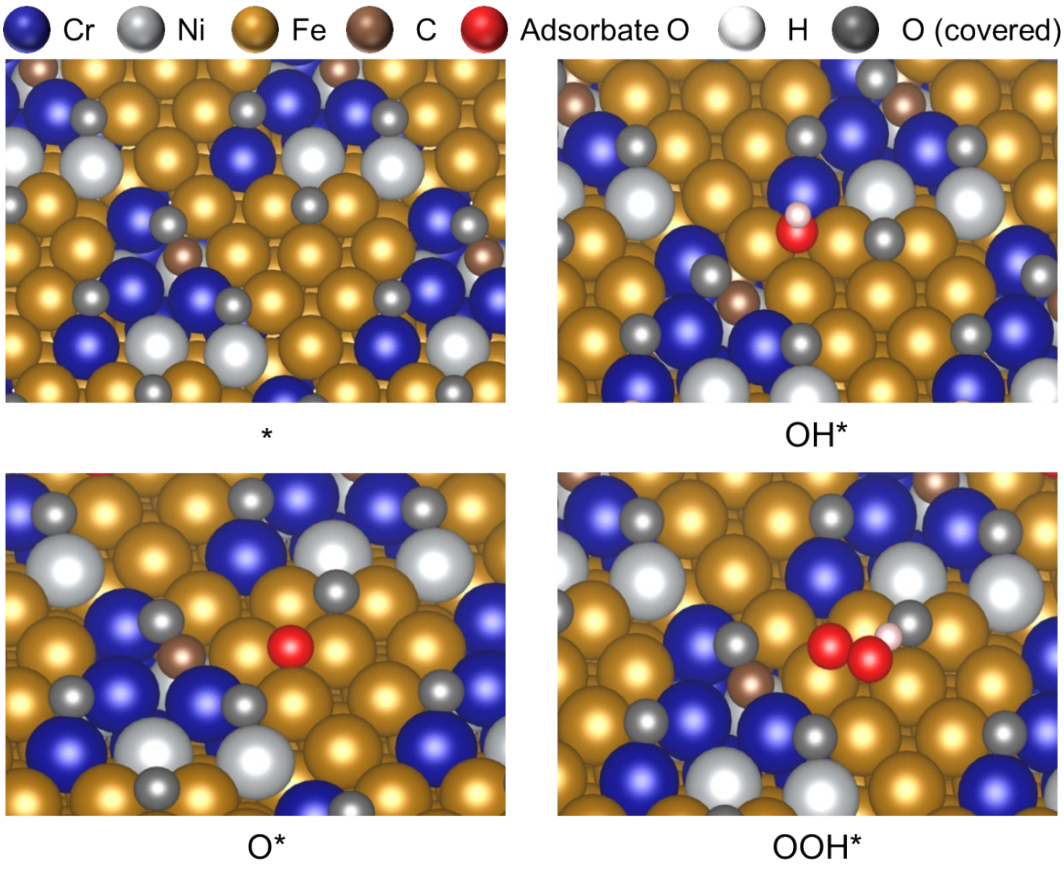

Fig. S14 DFT The reaction diagram of the stainless steel body.

Table S6 ICP-OES results of the 316L-15 sample.

Samples	Measured atomic ratios (%)			
	Fe	Ni	Mn	Mo
316L-15	55.03	44.86	0.11	0.00

Table S7 The solubility of the metal hydroxides (Fe, Ni, Mn)（wt.%）.

Chemical Formula	**$Fe(OH)_3$**	**$Fe(OH)_2$**	**$Ni(OH)_2$**	**$Mn(OH)_2$**
K_{sp}	3.2×10^{-28}	1.0×10^{-15}	2.0×10^{-15}	1.1×10^{-13}

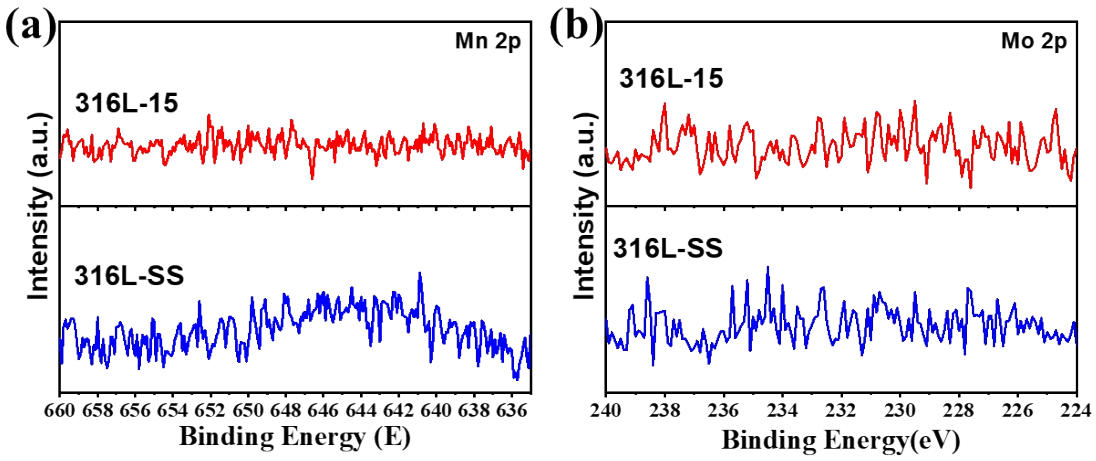

Fig. S15 High-resolution XPS spectra of (a) Mn 2p and (b) Mo 2p for the 316-SS and 316-15.

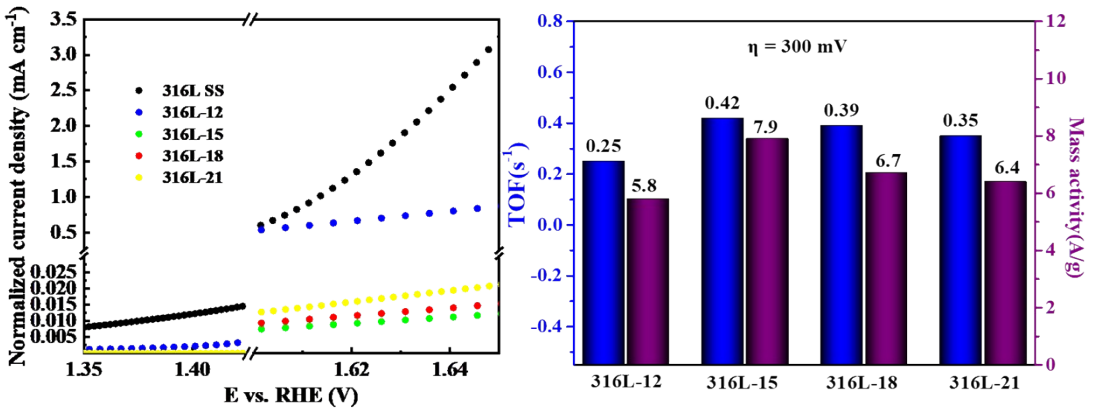

Fig. S16 (a)Normalized current density by the ECSA and (b)Mass activity and TOF values of the 316L-12, 316L-15, 316L-18 and 316L-21 at the overpotential of 300 mV.

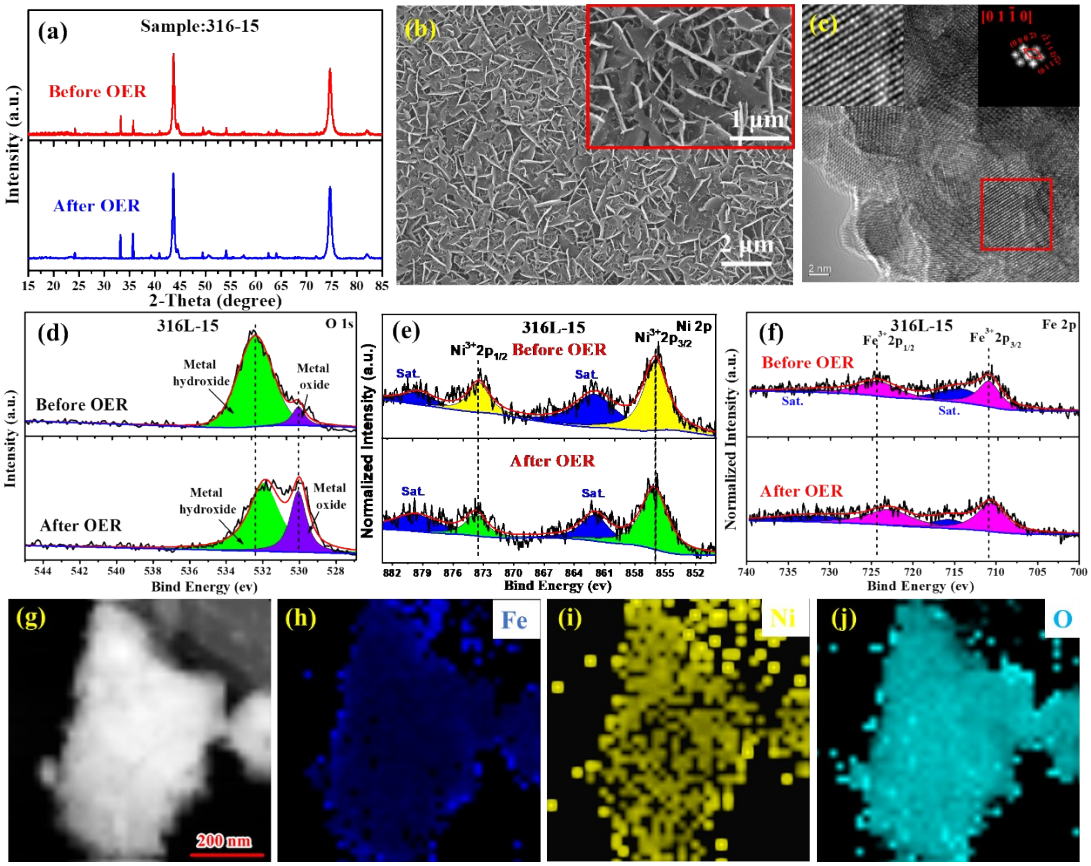

Fig. S17 (a) XRD patterns of 316L-15 before and after OER. (b) Low and high(inset) magnification SEM images (c) HRTEM images (inset: the corresponding fast Fourier transform (FFT) pattern) of 316L-15 after OER. (d-f) High-resolution of XPS spectra of (d)O 1s, (e)Ni 2p, and (f)Fe 2p of 316L-15 before and after OER. (g-j) EDX element mapping images of 316L-15 after OER.